Kedare et al. 2015. *Int. J. Vehicle Structures & Systems*, 7(1), 25-30
ISSN: 0975-3060 (Print), 0975-3540 (Online)
doi: 10.4273/ijvss.7.1.05

International Journal of Vehicle Structures & Systems
Available online at www.maftree.org/eja

Computational Fluid Dynamics Analysis of Empty Railway Freight Wagons

Shashank B. Kedare[a], S.C. Sharma[b] and S.P. Harsha[c]

Mechanical & Industrial Engg. Dept., Indian Institute of Technology, Roorkee, India
[a]*Corresponding Author, Email: kedareshashank@gmail.com*
[b]*Email: sshmefme@iitr.ac.in*
[c]*Email: spharsha@gmail.com*

ABSTRACT:

Increase in the speed of train leads to aerodynamic problems. These problems occur due to turbulent behaviour of air flow around the train. So it is of great concern to study the dynamics of fluid flow. This paper deals with the dynamic analysis of empty freight wagons due to air turbulence using computational fluid dynamics. The effect of important aerodynamic coefficients such as aerodynamic drag, pressure distribution and velocity stream line has been studied on realistic and simplified freight train geometries. The geometry is a scaled model of freight open wagon type'BOXN25' from Indian Railways. The aerodynamic analysis for empty wagons shows that the critical stress zone and the air drag effect are comparable between the two considered geometries.

KEYWORDS:

Aerodynamic drag; Computational fluid dynamics; Turbulence; Freight wagon

CITATION:

S.B. Kedare, S.C. Sharma and S.P. Harsha. 2015. Computational Fluid Dynamics Analysis of Empty Railway Freight Wagons, *Int. J. Vehicle Structures & Systems*, 7(1), 25-30. doi:10.4273/ijvss.7.1.05.

ACRONYMS AND NOMENCLATURE:

ρ	*Density (kg/m^3)*
τ_{ij}	*Stress Tensor*
S_{ij}	*Strain Tensor*
$\bar{u}(u,v,w)$	*Flow velocity vector (m/s)*
$\overline{U}(U_i,U_j)$	*Mean flow velocity (m/s)*
$\bar{u}'(u_i',u_j')$	*Fluctuating mean velocity (m/s)*
$\bar{f}(f_x,f_y,f_z)$	*Body force per unit mass (N)*

1. Introduction

Train travel is an efficient transportation in comparison to other ways of transportation. Transport is viewed as one of the critical infrastructures for the economy. In national transport systems, freight transport acts as the critical link between ports, markets and manufacturing centres. As largest employer of the country, Indian Railways acts as socio-economical catalyst in the economic development. Freight trains are integral part of the Indian Railways. Indian freight railway carries nearly 1000 million tonnes of freight in a year. Freight trains bring two third of revenue for Indian Railways and referred as its bread earner. Considering high growth in the freight traffic for coming years there is recognition among policymakers in India to introduce dedicated fright corridors, high speed trains and increase in the speed of existing trains [14]. With increase in the operating speed of the train the issues related to the aerodynamic force, moments, stability of vehicle, aerodynamic noise, and operational safety have to be addressed. However, to speed up the train much effort has been paid to increase the power requirement rather than understanding the physical air flow around the train. This led to larger energy losses and performance deterioration of train. The aerodynamic forces are proportional to square of velocity due to which much of energy is being lost in overcoming force called drag force. More research has been done to reduce aerodynamic drag of high speed trains. The freight-trains used in India and the rest of world today are relatively old and do not have an appropriate aerodynamic design. So it is of great concern to study the dynamic behaviour of fluid flow around the freight train.

For the purpose of development of a faster and safer train system with lower air pollution and noise, many researchers are paying much attention on the aerodynamics of train. Biadgo and Simnovic [1] studied the flow around ICE-2 high speed train for different yaw angles using Reynolds-Averaged Navier-Stokes (RANS) equations. The computed aerodynamic coefficients were in good agreement with experimental results. Paul [12] studied the distance between the wagons in a freight train which significantly affects the drag coefficient of each wagon and found that as the gap between two wagon increases, the aerodynamic drag also increases and vice versa. As the gap size increases, the shear layers start to interact with the re-circulating flow in the gap and more momentum is transferred from the surrounding air to the wagon and thus the drag increases. Horner [11] found that the drag of the freight wagon can be reduced by as much as 15% by smoothing the sides of containers. Sharma [4-7] studied performance characteristics such as lateral stability, curving, multibody simulation, wheel to track interaction, ride quality, comfort and analysed critical parameter which influences railway vehicle dynamic stability.

Mohebbi and Rezvani [3] studied aerodynamic performance of regional passenger train under cross wind. The results depict that coefficient of drag, side force and yaw moment for any yaw angle is independent of Reynolds's number. Decreasing the gap between the car decreases drag coefficient. Variation in the car gap did not show any significant effect. Browand and Hamache [9-10] studied the drag coefficient of a closed type freight wagon depending on its position in the train. The drag coefficient after the first 3-4 wagons will reach value that are 20-50% lesser than the drag coefficient of the first wagon. The contribution to the total drag of the entire train from the locomotive will in turn be higher than the drag of the first wagon due to the stagnation pressure of the air on the front of the locomotive and the low pressure region in the wake of the locomotive. Sterling [8] compared various full-scale and model scale experiments that have been carried out with high speed passenger and freight trains to study the characteristics of slip streams. The purpose of the study was to understand the flow structure in the different regions like nose, boundary layer and near wake, so that the difficulties caused to the passengers and trackside workers could be figured out. When comparing the different regions of the flow, the magnitude and duration of the peak gusts in the slip stream were examined. In the up-stream, a localized velocity peak is observed but is much smaller than the velocity peaks that exist in the boundary layer and near wake regions. The duration of the velocity peak is also small and thereby concluded that this region does not pose any danger to the passengers or trackside workers.

Osth [2] simulated the unsteady flow at zero yaw angles around a container freight wagon with two cases, one single wagon and one wagon submerged in a train set with a wagon in front of it and one wagon behind. The flow around the periodic wagon was found to be very different from the flow around the single wagon as expected. The presence of a wagon upstream and a wagon downstream removes all the areas on the wagon where flow impinges directly on the front of the wagon and thus the areas of massive separated flow on the roof and on the side of the wagon were observed. The gap between the wagons was found to contain two counter rotating vortices that are symmetric. This paper deals with the dynamic analysis of empty freight wagons due to air turbulence using computational fluid dynamics (CFD). The effect of important aerodynamic coefficients such as aerodynamic drag, pressure distribution and velocity stream line has been studied on realistic and simplified freight train geometries. The geometry is a scaled model of freight open wagon type'BOXN25' from Indian Railways. The critical stress zone and the air drag effect between the two considered geometries are compared using ANSYS Fluent CFD software.

2. Aerodynamic theory

The continuity equation and Navier-Stokes equation are the governing equations to study the flow behaviour. These governing equations will be derived using fundamental principles such as conservation of mass and Newton's second law.

The continuity equations for compressible flow [15] are given by,

$$\frac{D}{Dt}\int_0^v \rho dV = 0 \tag{1}$$

$$\frac{\partial \rho}{\partial t} + \nabla \cdot \left(\rho \cdot \bar{u}\right) = 0 \tag{2}$$

A dynamic equation which describes fluid motion can be obtained by applying Newton's second law to a particle. To derive the differential form of the momentum equation, Newton's second law as below is applied to an infinitesimal fluid particle of mass dm.

$$\bar{F} = \frac{\overline{dP}}{dt_{system}} \tag{3}$$

The forces acting on surface can be classified as surface force and body force. Let us consider *x* component of force acting on element of mass dm and volume *dv=dx dy dz* as shown in Fig. 1. When gravity force is only the body force acting on element, then the body force per unit mass is ĝ. The net force acting in x direction dFx is given by,

$$dF_x = dF_{bx} + dF_{sx} = \left(-\frac{dp}{dx} + \frac{d\tau_{xx}}{dx} + \frac{d\tau_{yx}}{dx} + \frac{d\tau_{xz}}{dx} + \rho f_x\right) dx\, dy\, dz \tag{4}$$

Applying Newton's second law in x, y and z directions,

$$\rho\frac{Du}{Dt} = -\frac{dp}{dx} + \frac{d\tau_{xx}}{dx} + \frac{d\tau_{yx}}{dx} + \frac{d\tau_{xz}}{dx} + \rho f_x \tag{5}$$

$$\rho\frac{Du}{Dt} = -\frac{dp}{dy} + \frac{d\tau_{xy}}{dy} + \frac{d\tau_{yy}}{dy} + \frac{d\tau_{yz}}{dy} + \rho f_y \tag{6}$$

$$\rho\frac{Du}{Dt} = -\frac{dp}{dz} + \frac{d\tau_{xz}}{dz} + \frac{d\tau_{zy}}{dz} + \frac{d\tau_{zz}}{dz} + \rho \tag{7}$$

Eqns. (5)-(7) are Navier-Stokes equations as,

$$\rho\frac{Du}{Dt} = \rho\frac{du}{dt} + \rho\bar{u}\cdot\nabla \tag{8}$$

$$\nabla\cdot\left(\rho u\bar{u}\right) = u\nabla\cdot\left(\rho\cdot\bar{u}\right) + \left(\rho\bar{u}\right)\cdot\nabla u \tag{9}$$

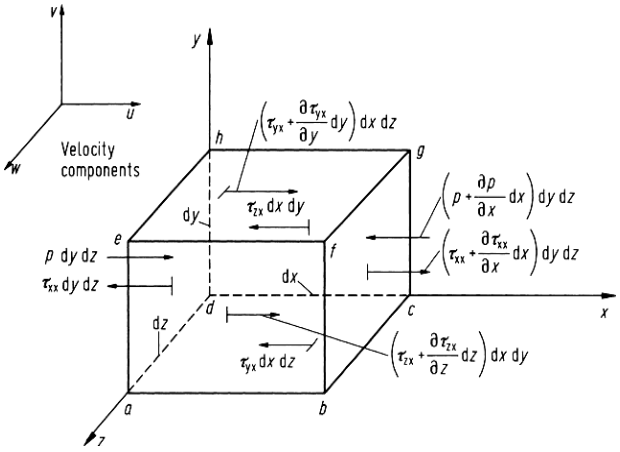

Fig. 1: Stresses in X direction of an element of fluid [1]

Recalling the vector identity for the divergence of the product of scalar times a vector, and combining with Eqn. (2), the resulting equations are,

$$\rho\frac{Du}{Dt}=\frac{\partial(\rho u)}{\partial t}-u\left(\frac{\partial\rho}{\partial t}+\nabla\cdot\left(\rho\bar{u}\right)\right)+\nabla\cdot\left(\rho u\bar{u}\right) \quad (10)$$

$$\rho\frac{Du}{Dt}=\frac{\partial(\rho u)}{\partial t}+\nabla\cdot\left(\rho u\bar{u}\right) \quad (11)$$

From Eqns. (11) and (5)-(7) Navier-Stokes equations [15] can be written as,

$$\frac{\partial(\rho u)}{\partial t}+\nabla\cdot\left(\rho u\bar{u}\right)=-\frac{dp}{dx}+\frac{d\tau_{xx}}{dx}+\frac{d\tau_{yx}}{dx}+\frac{d\tau_{xz}}{dx}+\rho f_x \quad (12)$$

$$\frac{\partial(\rho v)}{\partial t}+\nabla\cdot\left(\rho v\bar{u}\right)=-\frac{dp}{dy}+\frac{d\tau_{xy}}{dy}+\frac{d\tau_{yy}}{dy}+\frac{d\tau_{yz}}{dy}+\rho f_y \quad (13)$$

$$\frac{\partial(\rho w)}{\partial t}+\nabla\cdot\left(\rho w\bar{u}\right)=-\frac{dp}{dz}+\frac{d\tau_{xz}}{dz}+\frac{d\tau_{zy}}{dz}+\frac{d\tau_{zz}}{dz}+\rho f_z \quad (14)$$

Consider an incompressible flow, the equation for conservation mass and momentum are,

$$\partial u_i/\partial x_i=0 \quad (15)$$

$$\rho\frac{\partial u_i}{\partial t}+\rho u_j\frac{\partial u_i}{\partial x_j}=-\frac{\partial p}{\partial x_i}+\frac{\partial\tau_{ji}}{\partial x_j} \quad (16)$$

$$\tau_{ij}=2\mu s_{ij} \quad (17)$$

$$S_{ij}=\frac{1}{2}\left(\frac{\partial u_i}{\partial x_j}+\frac{\partial u_j}{\partial x_i}\right) \quad (18)$$

The Navier-Stokes theorem in convective form

$$\rho\frac{\partial u_i}{\partial t}+\rho\frac{\partial\left(u_i u_j\right)}{\partial x_j}=-\frac{\partial p}{\partial x_i}+\frac{\partial\left(2\mu S_{ij}\right)}{\partial x_j} \quad (19)$$

Time averaging Eqns. (15) and (19) we get,

$$\frac{\partial U_i}{\partial x_i}=0 \quad (20)$$

$$\rho\frac{\partial U_i}{\partial t}+\rho\frac{\partial\left(U_j U_i+\overline{u_j' u_i'}\right)}{\partial x_j}=-\frac{\partial p}{\partial x_i}+\frac{\partial\left(2\mu S_{ji}\right)}{\partial x_j} \quad (21)$$

In order to compute all mean properties of turbulent flow under consideration, we need prescription for computing $\overline{u_j' u_i'}$. Rearranging terms in Eqn. (21) we get:

$$\rho\frac{\partial U_i}{\partial t}+\rho U_j\frac{\partial U_i}{\partial x_j}=-\frac{\partial p}{\partial x_i}+\frac{\partial\left(2\mu S_{ji}-\rho\overline{u_j' u_i'}\right)}{\partial x_j} \quad (22)$$

The term $\rho\overline{u_j' u_i'}$ is known as Reynolds's stress tensor [17] as,

$$\tau_{ij}=-\rho\overline{u_j' u_i'} \quad (23)$$

Due to nonlinearity of Navier-Stokes equation if we take large moment we generate more number of unknowns as compared to number of equations. The function of turbulence modeling is to devise approximation for unknown correlation in terms of known flow properties so that sufficient number of equations exists [17] as,

$$\tau_{ij}=\begin{bmatrix}\overline{u'^2} & \overline{u'v'} & \overline{u'w'}\\ \overline{v'u'} & \overline{v'^2} & \overline{v'w'}\\ \overline{w'u'} & \overline{w'v'} & \overline{w'^2}\end{bmatrix} \quad (24)$$

The two-equation eddy viscosity model, specifically the realizable k-∈ turbulence model, is found effective closer to the nonlinear equations in Eqn. (24).

$$\rho\overline{u_j' u_i'}=\mu_t\left(\frac{\partial u_i}{\partial x_j}+\frac{\partial u_j}{\partial x_i}\right)-\frac{2}{3}\delta_{ij}\left(\mu_t\frac{\overline{\partial\mu_k}}{\partial x_k}-\rho k\right) \quad (25)$$

Where k is turbulent kinetic energy. The k-∈ model considers the effect of turbulence kinetic energy [1, 15, and 16] using turbulence viscosity $\mu_t=\rho C_\mu k^2/\in$. Where C_μ is Constant. The transport equation for realizable k-∈ model can be expressed as,

$$\rho\frac{\partial k}{\partial t}+\rho\overline{u}_j\frac{\partial k}{\partial x_j}=\frac{\partial}{\partial x_j}\left[\left(\mu+\frac{\mu_t}{\sigma_k}\right)\frac{\partial k}{\partial x_j}\right]+P_k-\rho\in \quad (26)$$

$$\rho\frac{\partial\in}{\partial t}+\rho\overline{u}_j\frac{\partial\in}{\partial x_j}=\frac{\partial}{\partial x_j}\left[\left(\mu+\frac{\mu_t}{\sigma_\in}\right)\frac{\partial\in}{\partial x_j}\right]+\rho C_1 S\in-\rho C_2\frac{\in^2}{k+\sqrt{v\in}} \quad (27)$$

3. Modeling and boundary conditions

The simulation scenario consists of stationary freight wagon subjected to wind velocity of 27 m/s at zero yaw angles. To study the dynamics of fluid flow by means of numerical simulation, commercial CFD software ANSYS FLUENT 14.0 was used. Full sized geometries are generally not used for the aerodynamic analysis due to space constraint in wind tunnel for experimentation, computational time and geometrical complexities. Considering the numerical simulation for complete train requiring advanced computational than those available scaled geometries are used. In addition, since the flow structure downstream at certain distance from the nose of the train (less than one coach length) is more or less constant, a decrease in length does not alter the essential physical features of the flow. The two cases studied in this paper are comparison between realistic and simplified freight train geometry as shown in Fig. 2 and Fig. 3 respectively. Both geometries are of Indian railway freight open wagon type named 'BOXN25' constructed with the scale of 1:50 by using 'SOLIDWORKS' modeling software. Two wagons one preceding other is considered for the analysis purpose. Each wagon has 202 mm length, 64 mm width and 55 mm height. The stiffeners on side walls are considered in the realized geometry case while simplified geometry case neglects the side stiffener walls and assumed it to be smooth to compare their effect on the aerodynamic coefficient. Once the geometry of freight train has been created, a rectangular computational domain of sufficient size has been modelled and illustrated in Fig. 4.

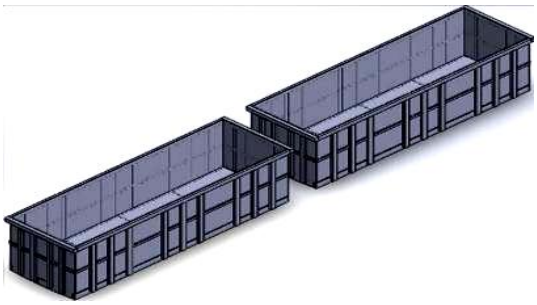

Fig. 2: Realistic freight wagon geometry

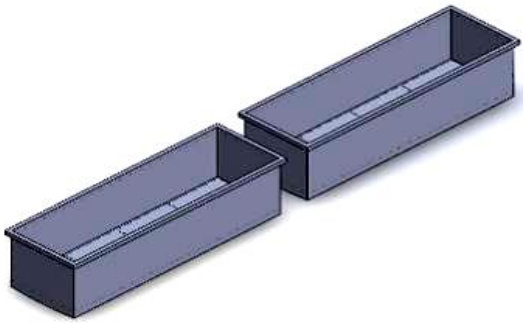

Fig. 3: Simplified freight wagon geometry

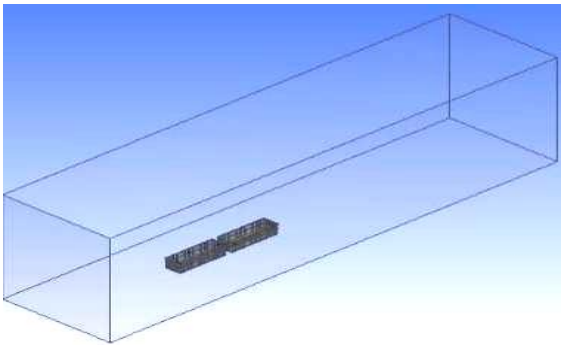

Fig. 4: Computational domain

The distance between train geometry and velocity inlet is kept such that it ensures the incoming flow will be with uniform velocity and pressure fields by the time when it reaches to the train. The computational domain is made sufficiently large to reduce the near wall effects. Mesh has been generated using tetrahedron element with patch confirming method. Face refinements has been given to the bogies. Inflation layer is provided at wagon and track to catch boundary layer effects. The mesh is generated with 2100287 elements. For better mesh resolution, each wall adjacent cell's centre should be located within log law layer, 30<y+ <300. A cross-section of mesh is shown in Fig. 5.

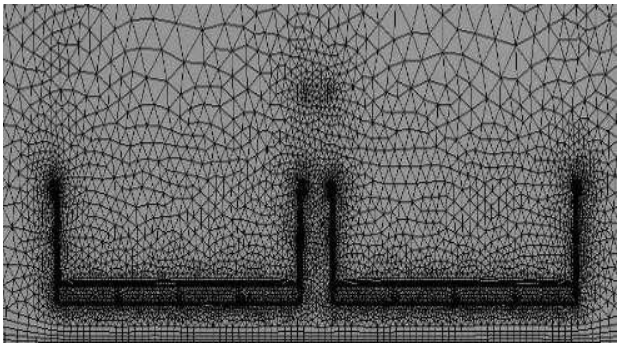

Fig. 5: Mesh cross section

The air with speed of 27 m/s was given as inlet boundary condition. At the outlet uniform Neumann boundary condition was applied i.e. pressure gradient equals to zero. This allows the flow to pass through the outlet without affecting the upstream flow provided that the upstream distance to the aerodynamic body is large enough. No-slip wall boundary conditions were applied to wagon surface and track assuming zero velocity at wall surface. Symmetric boundary conditions were used at side and top wall of computational domain considering the fact that zero shear slip wall in viscous flow. Due to the large application in automotive industry, the realizable k-∈ with non equilibrium wall treatment turbulence model was used for turbulence modeling. The incoming flow with turbulence intensity and viscosity ratio were set to 1% and 10 respectively. The backflow turbulence intensity and viscosity ratio were set to 5% and 10 respectively [1].

4. Results and discussion

The nature of the flow around the train subjected to zero yaw angles is studied in this paper. The aerodynamic coefficients of drag (Cd) for realistic and simplified freight geometry are shown in Fig. 6. The coefficient of drag was reduced by around 22% [12]. A possible reason for the higher coefficient of drag was geometry of train considered in the first case is more realistic and considers all complex parts in the analysis which increase the total surface area compared to the simplified geometries. Also the y+ criteria as shown in Fig. 7 and Fig. 8 respectively for realistic and simplified geometries were not completely fulfilled due to geometrical complexities. The reduction in C_d is due to reduction in area [12, 13]. When the size of edges is chamfered or rounded, the separation region disappears and value of C_d decreases considerably [13].

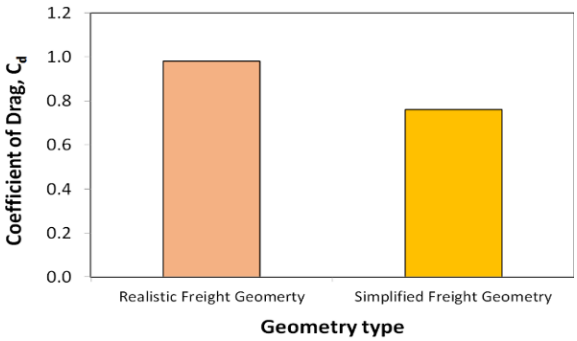

Fig. 6: Comparison of coefficient of drag

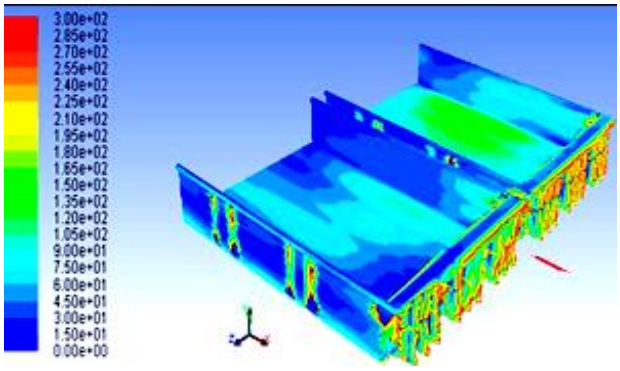

Fig. 7: Wall Y+contour for realistic wagon geometry

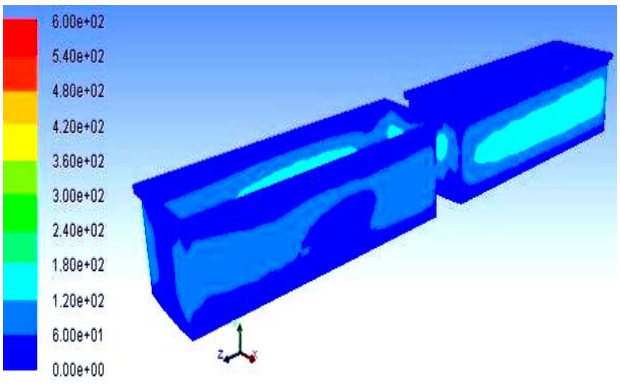

Fig. 8: Wall Y+contour for simplified wagon geometry

The coefficient of pressure contours as in Fig. 9 depicts that max. pressure occurs at the front end of wagon. It was due to the fact that wagon is kept at zero degree yaw angle and all the kinetic energy of incoming air was converted into pressure energy. The dimensionless pressure coefficient (Cp) for the front end was around '1'. The Cp for region behind the front end changes from being almost zero to negative. A Cp value of almost '1' refers to measured stagnation pressure. The mentioned area at the front indicates the separation region and change in flow direction. The presence of wagon at the front causes flow to impinge directly on the wagon front and thus causes massive flow separation at the top of the front wagon as shown in Fig. 10. An empty wagon provided enough space for the flow to re-circulate and cause vortex at the top. The gap between the wagons was found to contain a counter rotating vortices. These vortices effectively shield the gap from the separating shear layers from the upstream wagon and carry it over the gap where it re-attaches on the top sides of the next wagon. It was found that the flow in the gap oscillates in the lateral direction which causes the shear layers to impinge on the outermost parts of the downstream wagon face [10]. Similar kind of vortices are found in rear wake region as shown in Fig. 11.

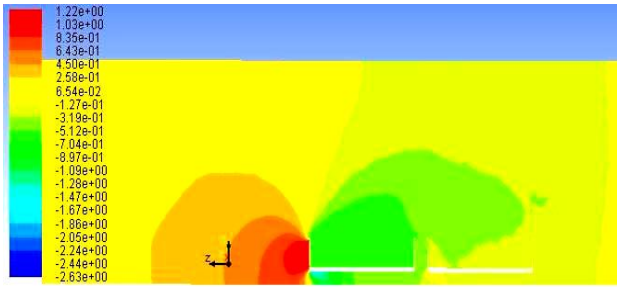

Fig. 9: Contour of coefficient of pressure

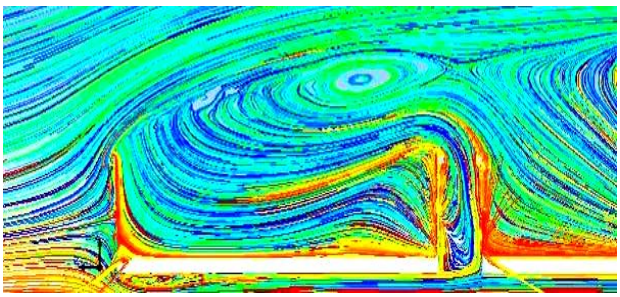

Fig. 10: Vortex at front wagon

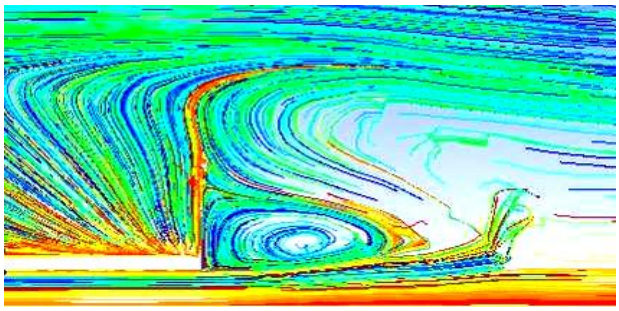

Fig. 11: Vortex at rear wake

The flow in the wake of three-dimensional bluff bodies is more complex due to the additional two shear layers emanating from the lateral sides of the body and more degrees of freedom. The time-averaged flow in the near wake of a three-dimensional bluff body consists of a ring vortex which is formed by the four separating shear layers. The flow appeared to be very complex. It shows how flow separates from the front leading edge and the flow behaviour through the side walls. Similar to the above observations, the vortices are generated at the side wall of the wagon mainly due to presence of side coping bars and stiffener bars. The vortex magnitude is higher at the front coping where large flow separation is occurring. The flow appeared to be pushed through the under carriage of wagon. The turbulence intensity comparison between two cases as shown in Fig. 12 and Fig. 13 depicts that turbulence intensity of realistic geometry is more compared to simplified case. The turbulence and vortices as shown in Figs. 14-16 are generated at the side wall of the wagon mainly due to presence of side coping bars and stiffener bars. The flow remains smooth for realistic geometry. The vortex magnitude is higher at the front where large flow separation is occurring. No considerable turbulence pattern is observed for simplified geometry due to neglecting side stiffener bars.

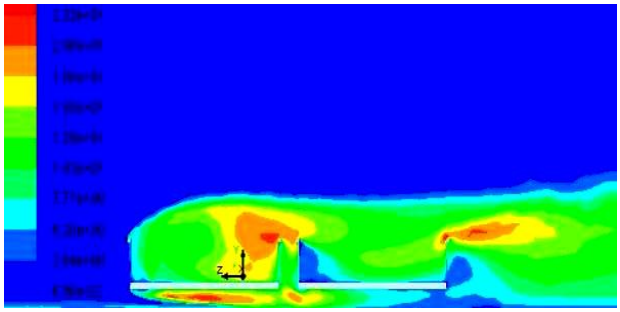

Fig. 12: Turbulence intensity for simplified geometry

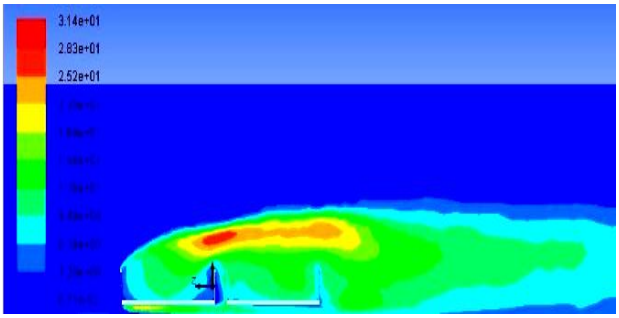

Fig. 13: Turbulence intensity for realistic geometry

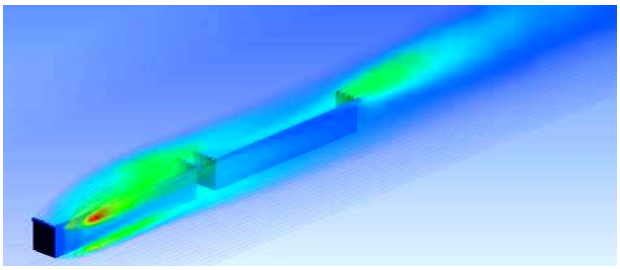

Fig. 14: Turbulence pattern

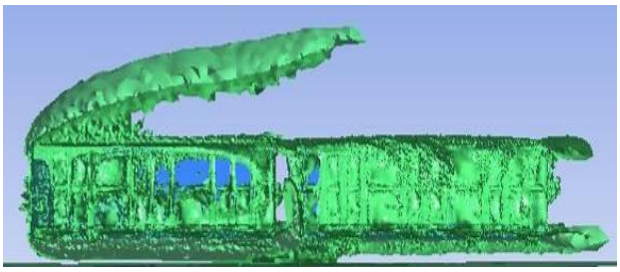

Fig. 15: Vortex region for realistic geometry

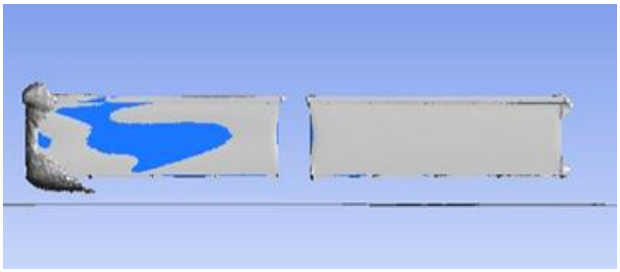

Fig. 16: Vortex region for simplified geometry

5. Conclusions

The turbulent flow behaviour of air has been studied and compared between the realistic and simplified geometry of Indian Railways freight wagon 'BOXN 25'. The aerodynamic parameters as drag coefficient, pressure distribution and velocity stream line have been studied. The simulation is done at static ground condition with zero yaw angles. The computed aerodynamic coefficients using realizable k-$\in$ and non equilibrium wall function are in good agreement with the reference studies. The critical turbulence prone areas and the effect of aerodynamic coefficient on the turbulence were shown. The coefficient of drag for simplified geometry is found to be much lower than the realistic geometry. Turbulence behaviour of realistic geometry is found to be much complex than the simplified geometry.

REFERENCES:

[1] A.M. Biadgo and A. Simnovic. 2014. Aerodynamic characteristics of high speed train under turbulent cross winds: A numerical investigation using unsteady-RANS method, *FME Trans.*, 42(1), 10-18. http://dx.doi.org/10.5937/fmet1401010B.

[2] J. Osth. 2013. A study of the aerodynamics of a generic container freight wagon using large-eddy simulation, *J. Fluids and Structures*, 44(5), 31-51.

[3] M. Mohebbi and M. Ali Rezvani. 2013. Numerical analysis of aerodynamic performance of regional passenger train under cross wind conditions, *Int. J. Vehicle Structure & Systems*, 5(2), 68-74. http://dx.doi.org/10.4273/ijvss.5.2.05.

[4] R.C. Sharma. 2013. Stability and Eigenvalue analysis of an Indian Railway general sleeper coach using Lagrangian dynamics, *Int. J. Vehicle Structures & Systems*, 5(1), 9-14. http://dx.doi.org/10.4273/ijvss.5.1.02.

[5] R.C. Sharma. 2012. Recent advances in railway vehicle dynamics, *Int. J. Vehicle Structures & Systems*, 4(2), 52-63. http://dx.doi.org/10.4273/ijvss.4.2.04.

[6] R.C. Sharma. 2011. Parametric analysis of rail vehicle parameters influencing ride behaviour, *Int. J. Engg. Sci. & Tech*, 3(8), 54-65.

[7] R.C. Sharma. 2011. Ride analysis of an Indian Railway coach using Lagrangian dynamics, *Int. J. Vehicle Structures & Systems*, 3(4), 219-224. http://dx.doi.org/10.4273/ijvss.3.4.02.

[8] M. Sterling. 2008. A study of the slipstreams of high-speed passenger trains and freight trains, *Proc. IMechE: J. Rail & Rapid Transit*, 222, 177-193. http://dx.doi.org/10.1243/09544097JRRT133.

[9] F. Browand and M. Hamache. 2004. The limits of drag behavior for two bluff bodies in tandem, *SAE Paper*, 8(3), 01-1145.

[10] F. Browand and M. Hamache. 1999. Aerodynamic forces experienced by a 3-vehicle platoon in a crosswind, *SAE Paper*, 1(2), 01-1324.

[11] S. Horner. 1965. Efficiency of Railroad Trains, *in Fluid Dynamic Drag. Horner Fluid dynamics*, 10-14.

[12] J. Paul. 2007. Application of CFD to rail car and locomotive aerodynamics, *The Aerodynamics of Heavy Vehicles II: Trucks, Buses, and Trains*, 1, 305-315.

[13] Y. Sakuma and A. Ido. 2009. Wind tunnel experiments on reducing separated flow region around front, *Quarterly Report of Railway Technical Institute*, 50.

[14] P. Pangotra. 2012. *Infrastructure for Low-Carbon Transport in India, A Case Study of the Delhi-Mumbai Dedicated Freight Corridor*, Magnum Custom Publishing, New Delhi.

[15] J. Philip. 2011. *Introduction to Fluid Mechanics*, John Wiley & Sons, USA.

[16] D.C. Wilcox. 2006. Turbulence modelling for CFD, *La Canada*, 3rd Edition, DCW Industries.

[17] J. Blazek. 2001. *Computational Fluid Dynamics: Principles and Applications*, Elsevier Science, Oxford.

EDITORIAL NOTES:

Edited paper from International Conference on Newest Drift in Mechanical Engineering, 20-21 December 2014, Mullana, Ambala, India.

GUEST EDITOR: Dr. R.C. Sharma, Dept. of Mech. Engg., Maharishi Markandeshwar University, Mullana, India.